Ocean inherent optical property determination from in-water light field measurements

Robert A. Leathers, Collin S. Roesler, and Norman J. McCormick

An algorithm is described and evaluated for determining the absorption and backscattering coefficients $a(z)$ and $b_b(z)$ from measurements of the nadir-viewing radiance $L_u(z)$ and downward irradiance $E_d(z)$. The method, derived from radiative transfer theory, is similar to a previously proposed one for $E_u(z)$ and $E_d(z)$, and both methods are demonstrated with numerical simulations and field data. Numerical simulations and a sensitivity analysis show that good estimates of $a(z)$ and $b_b(z)$ can be obtained if the assumed scattering phase function is approximately correct. In an experiment in Long Island Sound, estimates of $a(z)$ derived with these methods agreed well with those obtained from an *in situ* reflecting tube instrument.

OCIS codes: 010.4450, 030.5620, 160.4760, 290.3200, 290.1350.

1. Introduction

The estimation of the beam absorption and backscattering coefficients a and b_b of natural waters is a primary goal of optical oceanographers. These inherent optical properties (IOP's) determine the ocean surface color, the quality of underwater visibility, and the transfer rates of heat and photosynthetically available radiation into the upper ocean. The values of the IOP's depend on the type and concentration of the water components, primarily of phytoplankton, suspended sediment, and dissolved and particulate organic material. Therefore multispectral measurements of a and b_b can be used to determine the water constituent types and abundances. The values of a and b_b can be estimated from remote-sensing measurements of ocean color; however, *in situ* determinations are more accurate and are required for the development and verification of remote-sensing algorithms.

There are two general approaches to *in situ* IOP determination. The first is to measure the attenuation of an active light source through a water sample with an instrument that physically isolates the water sample from the surrounding environment.[1,2] The most widely used of these instruments is the ac-9 (WetLabs, Inc., Philomath, Oregon), which is capable of measuring fine-scale vertical variations in the IOP's and can operate day or night, within or below the euphotic zone. It has the disadvantages, though, that corrections must be made to the estimates of a to reduce scattering errors and that the volume of the sample is smaller than what is desired for most oceanographic applications. Also, the small intakes of these instruments can break up or fail to collect large suspended aggregates that affect underwater visibility.

The second approach to IOP determination is to measure the natural light within the water column and invert the radiative transfer equation to calculate the values of a and b_b that are consistent with the observed light measurements. This requires that the effects on the light field of the desired IOP's be separated analytically or empirically (rather than physically) from the effects of the illumination, sea state, and bottom conditions. This approach enables one to obtain the water and light field properties from the same instrument, but it can be employed only during the day and in the upper layers of the ocean where there is sufficient natural illumination. With the algorithm presented here, each

When this research was performed, R. A. Leathers and N. J. McCormick were with the Department of Mechanical Engineering, University of Washington, Box 352600, Seattle, Washington 98195. R. A. Leathers is now with the Naval Research Laboratory, Code 7212, Washington, D.C. 20375. His e-mail address is leathers@rsd.nrl.navy.mil. C. S. Roesler was with the Department of Marine Sciences, University of Connecticut, 1084 Shennecossett Road, Groton, Connecticut 06340. She is now with the Bigelow Laboratory for Ocean Sciences, McKown Point, P.O. Box 475, West Boothbay Harbor, Maine 04575.

Received 9 November 1998; revised manuscript received 30 April 1999.

0003-6935/99/245096-08$15.00/0

IOP estimate is affected by an optically large volume of water surrounding the nominal location of the estimate. Therefore it is not possible to resolve the fine vertical structure of waters that have high spatial variability. Nonetheless, even in highly variable waters, the method can retrieve spatially averaged estimates of the IOP's that may be appropriate for remote sensing and other large-scale applications.

Because the two general approaches for IOP determination are independent of one another, it should be possible to demonstrate optical closure between the two. This is attempted here with data collected in Long Island Sound by comparing the estimates of $a(z)$ obtained from an ac-9 instrument with those obtained from measurements of the downward irradiance $E_d(z)$ and either the nadir-viewing radiance $L_u(z)$ or the upward irradiance $E_u(z)$ at several depths z.

The method for determining $a(z)$ and $b_b(z)$ from profiles of $E_d(z)$ and $E_u(z)$ has been reported previously.[3] The approach consists of estimating the local asymptotic values of the downward diffuse attenuation coefficient and the irradiance reflectance $K_\infty(z)$ and $R_\infty(z)$, respectively, and then calculating $a(z)$ and $b_b(z)$ from $K_\infty(z)$ and $R_\infty(z)$. The method was evaluated with numerical simulations and a sensitivity analysis. Here the algorithm is extended to allow use of $L_u(z)$ instead of $E_u(z)$ and is applied to both simulations and field data. Also it is shown that the iteration step of the algorithm (for determining the single-scattering albedo ω_0) can be replaced by a simple inversion of the one-to-one correspondence between ω_0 and R_∞ that exists for any given scattering phase function.

Gordon and Boynton[4,5] have presented an alternative method for the estimation of $a(z)$ and $b_b(z)$ from $E_d(z)$ and $E_u(z)$ or $L_u(z)$. With this method, estimates of $a(z)$ and $b_b(z)$ are used to compute profiles of $E_d(z)$ and $E_u(z)$ or $L_u(z)$ with a radiative transfer numerical code. The differences between the computed and the measured $E_d(z)$ and $E_u(z)$ or $L_u(z)$ are used to iteratively adjust $a(z)$ and $b_b(z)$ until an optimal solution is obtained. This approach is far more computationally intensive than the method described here because, with our method, no iteration is required. Also the method of Gordon and Boynton requires the surface conditions (illumination and sea state) as an input, whereas our method does not require surface information. Although this makes the Gordon and Boynton algorithm more complicated to apply, the additional information should make it more accurate than our algorithm at shallow optical depths. Both approaches can accommodate the effects of bottom reflectance in optically shallow waters.

Our L_u–E_d method is presented in Sections 2 and 3, and a sensitivity analysis and numerical testing of the method is given in Sections 4 and 5, respectively. The application of both the E_u–E_d and L_u–E_d algorithms to field data is demonstrated in Section 6, and a discussion is given in Section 7.

2. Basic Equations

We are interested in the azimuthally averaged radiance $L(z, \mu)$ (in units of W m^{-2} sr^{-1} nm^{-1}) that satisfies the integrodifferential radiative transfer equation

$$\mu \partial L(z, \mu)/\partial z + c(z)L(z, \mu) = b(z) \int_{-1}^{1} \tilde{\beta}(z, \mu, \mu')L(z,\mu')\mathrm{d}\mu', \quad (1)$$

where b and c (in units of inverse meters) are the beam scattering and attenuation coefficients, $\tilde{\beta}$ is the scattering phase function normalized such that $\int_{-1}^{1} \tilde{\beta}(\mu, 1)\mathrm{d}\mu = 1$, and μ is the cosine of the polar angle with respect to the downward depth z (in meters). All quantities in Eq. (1) are implicitly a function of wavelength. The backscattering coefficient b_b is related to b by

$$b_b = b \int_{-1}^{0} \tilde{\beta}(\mu, 1)\mathrm{d}\mu, \quad (2)$$

and the absorption coefficient is related to b and c by $a + b = c$.

The irradiance ratio $R(z)$ and radiance–irradiance ratio $R^L(z)$ are

$$R(z) = E_u(z)/E_d(z), \quad R^L(z) = L_u(z)/E_d(z), \quad (3)$$

where $L_u(z)$ is the upward radiance [$L_u(z) = L(z, -1)$] and $E_u(z)$ and $E_d(z)$ (in units of W m^{-2} nm^{-1}) are the upward and downward irradiances:

$$E_u(z) = 2\pi \int_{-1}^{0} |\mu| L(z, \mu)\mathrm{d}\mu,$$

$$E_d(z) = 2\pi \int_{0}^{1} \mu L(z, \mu)\mathrm{d}\mu. \quad (4)$$

The upward and downward diffuse attenuation coefficients $K_u(z)$ and $K_d(z)$ (in inverse meters) are defined by

$$K_u(z) = -\frac{\mathrm{d} \ln[E_u(z)]}{\mathrm{d}z}, \quad K_d(z) = -\frac{\mathrm{d} \ln[E_d(z)]}{\mathrm{d}z}, \quad (5)$$

and the diffuse attenuation coefficient for $L(z, \mu)$ is denoted by $K_L(z, \mu)$, with

$$K_L(z, -1) = -\frac{\mathrm{d} \ln[L_u(z)]}{\mathrm{d}z}. \quad (6)$$

At large optical depths in deep homogeneous waters with no internal sources, the values of $R(z)$, $R^L(z)$, and $K_d(z)$ approach the asymptotic values R_∞, $R_\infty{}^L$, and K_∞, respectively, that are IOP's of the water. Because R_∞, $R_\infty{}^L$, and K_∞ are IOP's, they can be defined mathematically in terms of a, b, and $\tilde{\beta}$. Therefore, although they cannot always be directly measured, they have physical meaning in any waters and are in general a function of depth. At a partic-

ular depth, a solution of the equations of radiative transfer yields the relationships[3,6]

$$R_\infty = \tilde{g}_1(-\nu_1)/\tilde{g}_1(\nu_1), \tag{7}$$

$$R_\infty^{\,L} = \phi(-\nu_1, 1)/\tilde{g}_1(\nu_1), \tag{8}$$

$$K_\infty = c/\nu_1, \tag{9}$$

where

$$\tilde{g}_1(\nu) = \int_0^1 \phi(\nu, \mu)\mu d\mu \tag{10}$$

and ν_1 is the largest positive eigenvalue corresponding to the eigenfunction $\phi(\nu_1, \mu)$ of Eq. (1). The values of ν_1 and $\phi(\nu_1, \mu)$ depend only on $\tilde{\beta}$ and the single-scattering albedo ω_0, where $\omega_0 = b/c$. Therefore Eqs. (7) and (8) are explicit expressions for R_∞ and $R_\infty^{\,L}$ in terms of $\tilde{\beta}$ and ω_0 and Eq. (9) is an explicit expression for K_∞ in terms of $\tilde{\beta}$, b, and c.

To evaluate ν_1 and $\phi(\nu_1, \mu)$ from $\tilde{\beta}$ and ω_0, the spatial and angular dependencies in Eq. (1) can be separated with the eigenmodes $L_j(z, \mu) = \phi(\pm\nu_j, \mu)\exp(\mp cz/\nu_j)$, and the scattering phase function can be expanded in Legendre polynomials, yielding

$$\tilde{\beta}(\mu, \mu') = \frac{1}{2}\sum_{n=0}^{M}(2n+1)f_n P_n(\mu)P_n(\mu'), \quad f_0 = 1, \tag{11}$$

where f_n are the expansion coefficients, $P_n(\mu)$ are the Legendre polynomials, and M is the degree of scattering anisotropy. It is then found that the discrete eigenfunctions satisfy[6]

$$\phi(\pm\nu_j, \mu) = \frac{\omega_0\nu_j}{2(\nu_j \mp \mu)}\sum_{n=0}^{M}(2n+1)f_n \times g_n(\pm\nu_j)P_n(\mu), \quad \nu_j > 1. \tag{12}$$

The Chandrasekhar polynomials[7] $g_n(\pm\nu_j)$ obey the recursion formula

$$ng_n(\nu_j) = h_{n-1}\nu_j g_{n-1}(\nu_j) - (n-1)g_{n-2}(\nu_j), \tag{13}$$

starting with $g_{-1} = 0$ and $g_0 = 1$, where $h_n = (2n + 1)(1 - \omega_0 f_n)$. From the spherical harmonics (P_N) method[8] with N odd and arbitrarily large, the positive eigenvalues ν_j are approximately the roots of

$$g_{N+1}(\nu_j) = 0. \tag{14}$$

3. Methods

Several steps are taken to estimate the values of $a(z)$ and $b_b(z)$ from field measurements of $L_u(z)$ and $E_d(z)$. First, to reduce noise, $L_u(z)$ and $E_d(z)$ are smoothed with respect to depth by making linear least-squares fits to $\ln[L_u(z)]$ and $\ln[E_d(z)]$ over small ranges of depths. Second, $R^L(z)$ and $K_d(z)$ are computed from these smoothed profiles with Eqs. (3) and (5).

The third step is the determination of $R_\infty^{\,L}(z)$ and $K_\infty(z)$ from $R^L(z)$ and $K_d(z)$. In optically deep and well-mixed waters, the profiles $R^L(z)$ and $K_d(z)$ asymptotically approach the values $R_\infty^{\,L}$ and K_∞. Therefore if it is known that the water is homogeneous and optically deep, then $R_\infty^{\,L}(z)$ and $K_\infty(z)$ are independent of depth and can be taken to be equal to the values of $R^L(z)$ and $K_d(z)$ deep in the euphotic zone. If the water is homogeneous but optically shallow with a highly absorbing bottom, then $R_\infty^{\,L}$ and K_∞ should be estimated from[3] $R_\infty^{\,L} \approx \max[R^L(z)]$ and $K_\infty \approx \max[K_d(z)]$. For optically shallow waters with a reflective bottom, an algorithm for the estimation of R_∞ is given in Ref. 3; however, an analogous equation for $R_\infty^{\,L}$ could not be derived in the same manner. In stratified waters, $R_\infty^{\,L}(z)$ and $K_\infty(z)$ are depth dependent and cannot be directly measured. However, $R_\infty^{\,L}(z)$ and $K_\infty(z)$ can be estimated with $R_\infty^{\,L}(z) \approx R^L(z)$ and $K_\infty(z) \approx K_d(z)$. Although these seemingly crude approximations are generally inaccurate near the surface and are not adequate to determine the fine vertical structure of highly stratified waters, they can give fairly accurate vertically smoothed profiles of the IOP's more than an optical depth from the surface.[3]

In the fourth step the values of $\omega_0(z)$ and $\nu_1(z)$ are calculated from $R_\infty^{\,L}(z)$. In Ref. 3, ω_0 was determined with an iterative solution method. However, this iterative technique is not necessary. There is a one-to-one correspondence between $R_\infty^{\,L}$ and ω_0 for a given $\tilde{\beta}$, and unique values of ν_1 follow from ω_0. Therefore, given the coefficients f_n of the assumed scattering phase function, a table can be generated of ν_1 and $R_\infty^{\,L}$ versus ω_0 with Eqs. (8), (10), and (12)–(14). This table can be inverted to obtain ω_0 and ν_1 versus $R_\infty^{\,L}$. For example, a plot of ω_0 and ν_1 versus $R_\infty^{\,L}$ for the Petzold scattering phase function[9] is shown in Fig. 1. Once these relationships are calculated, ω_0 and ν_1 can be quickly determined for any measured $R_\infty^{\,L}$.

Finally, from $\nu_1(z)$ and $\omega_0(z)$, the values of $c(z)$, $a(z)$, and $b(z)$ are calculated with $c(z) = \nu_1(z)K_\infty(z)$, $a(z) = c(z)[1 - \omega_0(z)]$, and $b(z) = c(z)\omega_0(z)$. The

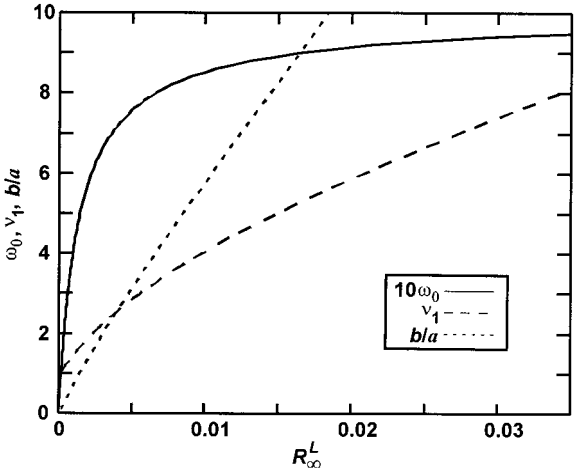

Fig. 1. Single-scattering albedo ω_0, the largest eigenvalue ν_1, and the ratio of scattering to absorption versus the asymptotic radiance–irradiance ratio $R_\infty^{\,L}$ for the Petzold scattering phase function.

values of $b_b(z)$ are computed from the substitution of Eqs. (11) into Eq. (2) to obtain[10]

$$b_b = (b/2)\sum_{n=0}^{M}(2n+1)f_n\int_{-1}^{0}P_n(\mu)\mathrm{d}\mu \tag{15}$$

$$= (b/2)\left[1-\sum_{n\ \mathrm{odd}}(2n+1)f_n\int_{0}^{1}P_n(\mu)\mathrm{d}\mu\right]. \tag{16}$$

4. Sensitivity Analysis

In practice, the accuracy of the L_u–E_d method depends on the sensitivities of a and b_b to small variations in K_∞ and $R_\infty{}^L$. The normalized sensitivity coefficients of a and b_b with respect to K_∞ are identically unity[3]:

$$\frac{K_\infty}{a}\frac{\partial a}{\partial K_\infty}=\frac{K_\infty}{b_b}\frac{\partial b_b}{\partial K_\infty}=1. \tag{17}$$

For example, a 1% increase in K_∞ results in a 1% increase in the calculated values of a and b_b. Analytical expressions for the sensitivity coefficients of a and b_b with respect to R_∞, expressed as functions of easily computed forward-problem sensitivity coefficients, were derived previously[3] for the E_u–E_d method. Those with respect to $R_\infty{}^L$ can be derived in the same manner, and the resulting expressions are the same except with R_∞ replaced by $R_\infty{}^L$:

$$\frac{R_\infty{}^L}{a}\frac{\partial a}{\partial R_\infty{}^L}=\left(\frac{R_\infty{}^L}{\nu_1}\frac{\partial \nu_1}{\partial R_\infty{}^L}\right)-\left(\frac{\omega_0}{1-\omega_0}\right)\left(\frac{R_\infty{}^L}{\omega_0}\frac{\partial \omega_0}{\partial R_\infty{}^L}\right), \tag{18}$$

$$\frac{R_\infty{}^L}{b_b}\frac{\partial b_b}{\partial R_\infty{}^L}=\left(\frac{R_\infty{}^L}{\nu_1}\frac{\partial \nu_1}{\partial R_\infty{}^L}\right)+\left(\frac{R_\infty{}^L}{\omega_0}\frac{\partial \omega_0}{\partial R_\infty{}^L}\right). \tag{19}$$

The forward-problem sensitivity coefficients $[(R_\infty{}^L/\nu_1)(\partial\nu_1/\mathrm{d}R_\infty{}^L)]$ and $[(R_\infty{}^L/\omega_0)(\partial\omega_0/\mathrm{d}R_\infty{}^L)]$ are always positive and can be evaluated from the numerical relationships shown in Fig. 1. It can be seen from Eqs. (18) and (19) that the effects of $(\mathrm{d}\nu_1/\mathrm{d}R_\infty{}^L)$ and $(\mathrm{d}\omega_0/\mathrm{d}R_\infty{}^L)$ on the estimation of b_b are additive, whereas the effects of these on the estimation of a tend to cancel. Therefore a is much less sensitive to $R_\infty{}^L$ than is b_b. Although the term $[\omega_0/(1-\omega_0)]$ in Eq. (18) is large for ω_0 near unity, it is multiplied by the term $(\partial\omega_0/\partial R_\infty{}^L)$ that is small for ω_0 near unity. Nonetheless the sensitivities of a and b_b to R_∞ and $R_\infty{}^L$ are much larger for ω_0 near unity than for $\omega_0 < 0.9$. The values of the sensitivity coefficients of Eqs. (18) and (19) are shown in Fig. 2 for the Petzold scattering phase function. Estimates of a are relatively insensitive to $R(z)$ and $R^L(z)$, with the magnitude of the sensitivity coefficients being less than 0.3 for $\omega_0 < 0.9$. Although b_b is somewhat more sensitive than a to R_∞ and $R_\infty{}^L$, $(R_\infty/b_b)(\partial b_b/\partial R_\infty) < 1$ for $\omega_0 < 0.980$ and $(R_\infty{}^L/b_b)(\partial b_b/\partial R_\infty{}^L) < 1$ for $\omega_0 < 0.988$. Both a and b_b are slightly less sensitive to R_∞ than to $R_\infty{}^L$ for $\omega_0 < 0.8$ and vice versa for $\omega_0 > 0.8$. As ω_0 approaches zero, the normalized sensitivity coefficients of a and b approach zero and unity, respectively.

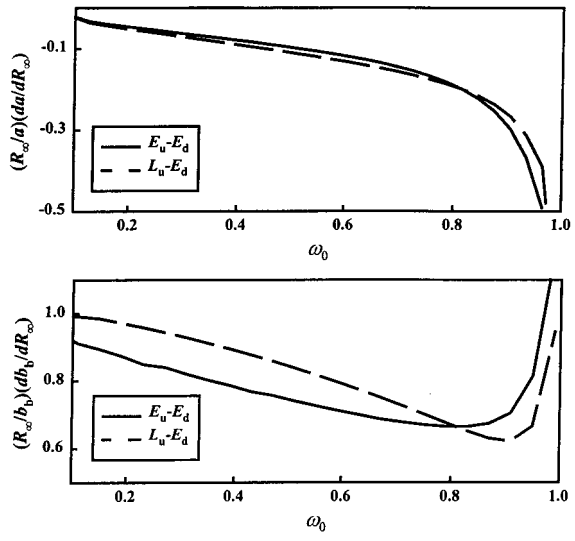

Fig. 2. Normalized sensitivity coefficients $(R_\infty/a)(\mathrm{d}a/\mathrm{d}R_\infty)$, $(R_\infty{}^L/a)(\mathrm{d}a/\mathrm{d}R_\infty{}^L)$, $(R_\infty/b_b)(\mathrm{d}b_b/\mathrm{d}R_\infty)$, and $(R_\infty{}^L/b_b)(\mathrm{d}b_b/\mathrm{d}R_\infty{}^L)$ for the Petzold scattering phase function.

Expressions were previously determined[3] for the sensitivity coefficients of a and b_b with respect to a parameter p of the scattering phase function. This parameter had been taken to be the scattering asymmetry factor but can be any scalar descriptor of the phase function. The sensitivity coefficients expressed in terms of the three forward-problem sensitivity coefficients are

$$\frac{p}{a}\frac{\partial a}{\partial p}=\left(\frac{p}{\nu_1}\frac{\partial \nu_1}{\partial p}\right)-\left(\frac{\omega_0}{1-\omega_0}\right)\left(\frac{p}{\omega_0}\frac{\partial \omega_0}{\partial p}\right), \tag{20}$$

$$\frac{p}{b_b}\frac{\partial b_b}{\partial p}=\frac{p}{\nu_1}\frac{\partial \nu_1}{\partial p}+\frac{p}{\omega_0}\frac{\partial \omega_0}{\partial_p}+\frac{p}{\tilde{b}_b}\frac{\partial \tilde{b}_b}{\partial p}, \tag{21}$$

where $\partial\omega_0/\partial p = (1/\partial R_\infty{}^L)(\partial R_\infty{}^L/\partial p)$. Estimates of a are insensitive to the scattering phase function,[3,4] as the effects of the sensitivities of ν_1 and ω_0 with respect to p in Eq. (20) tend to cancel. Therefore the accuracy of the assumed phase function is unimportant in the estimation of a. In the estimation of b_b, on the other hand, the effects of the sensitivities of ν_1 and ω_0 to p in Eq. (21) are additive. However, because these tend to have the opposite sign of the last term in Eq. (21), b_b is far less sensitive to the assumed $\tilde{\beta}$ than is b, for which the sensitivity coefficient is similar to Eq. (21) but with the last term absent.[3] For the estimation of b_b, the most important parameter describing the assumed scattering phase function is $\tilde{b}_b = b_b/b$. If p is taken to be $\tilde{b}_b$, then Eq. (21) becomes

$$\frac{\tilde{b}_b}{b_b}\frac{\partial b_b}{\partial \tilde{b}_b}=\frac{\tilde{b}_b}{\nu_1}\frac{\partial \nu_1}{\partial \tilde{b}_b}+\frac{\tilde{b}_b}{\omega_0}\frac{\partial \omega_0}{\partial \tilde{b}_b}+1. \tag{22}$$

Because for a given measurement of $R_\infty{}^L$ an overestimate of $\tilde{b}_b$ leads to an underestimate of ω_0 and ν_1, and vice versa, the terms $(\partial\nu_1/\partial\tilde{b}_b)$ and $(\partial\omega_0/\partial\tilde{b}_b)$ in Eq. (22) are negative and tend to cancel with the

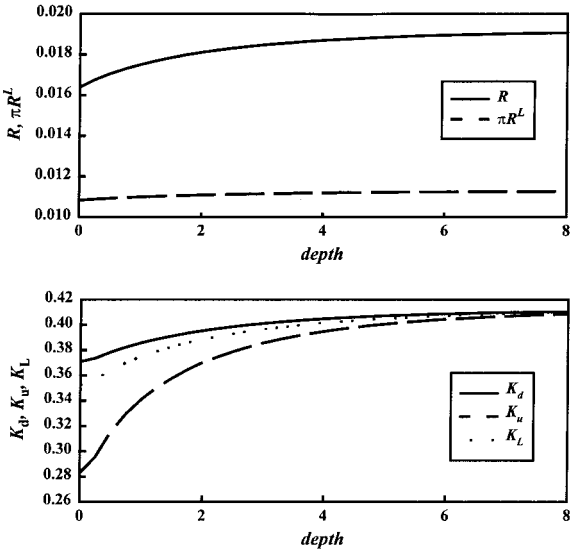

Fig. 3. Simulated profiles of the irradiance and radiance–irradiance ratios and of the diffuse attenuation coefficients for the case of homogeneous optically deep water with $a = 0.30$, $b = 0.70$, a flat surface, and an illumination that is 30% diffuse skylight and 70% direct sunlight at 30° from the zenith.

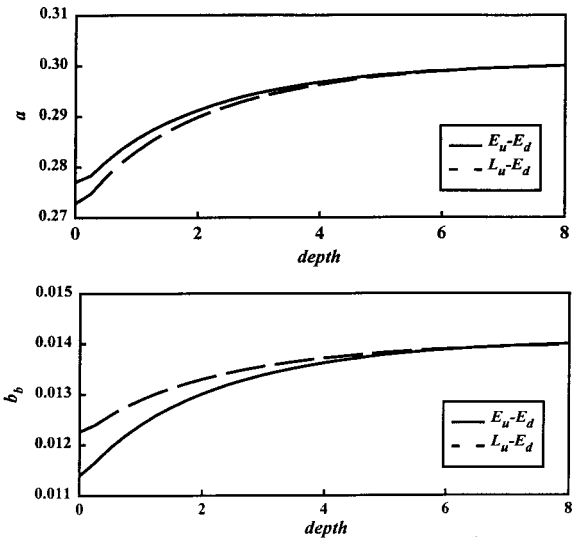

Fig. 4. Estimates of the absorption and backscattering coefficients for the simulation of Fig. 3 obtained with the E_u–E_d and L_u–E_d methods.

unity term. Therefore, although the accurate determination of b_b requires that $\tilde{b}_b$ of the assumed scattering phase function be approximately that of the true scattering phase function, b_b is not too sensitive to the assumed $\tilde{b}_b$ to make its estimation impractical.[3,5]

5. Numerical Simulations

Numerical simulations were performed to evaluate the L_u–E_d method for determining $a(z)$ and $b_b(z)$ and to compare this method's performance with that of the E_u–E_d algorithm. Simulated $L_u(z)$, $E_u(z)$, and $E_d(z)$ data were generated for the San Diego Harbor Petzold scattering phase function[11] and specified $\omega_0(z)$, surface roughness, and illumination conditions. Simulations for flat, homogeneous waters were performed with the discrete ordinates radiative transfer code DISORT,[12] whereas data for roughened surfaces or inhomogeneous waters were generated with Hydrolight.[13]

For example, shown in Fig. 3 are $\pi R^L(z)$, $R(z)$, $K_d(z)$, $K_u(z)$, and $K_L(z, -1)$ for the case of homogeneous optically deep water with $a = 0.30$, $b = 0.70$ ($b_b = 0.014$), a flat surface, and an illumination that is 30% diffuse skylight and 70% direct sunlight at 30° from the zenith. The values all increased nearly monotonically with depth. Those of $\pi R^L(z)$ and $R(z)$ approached their respective asymptotic values of 0.011 and 0.019. As was found in general for simulations over a wide range of illumination conditions and water optical properties, the profile of $R^L(z)$ was much more constant with depth than $R(z)$ and therefore closer than $R(z)$ to its respective asymptotic value. The profiles $K_d(z)$, $K_u(z)$, and $K_L(z, -1)$ approached their shared asymptotic value of 0.41, with $K_d(z)$ being closest to K_∞. At large depths the values of K_∞, $R_\infty{}^L$, and R_∞ can be measured directly with high accuracy. Therefore if the waters are known to be homogeneous, the depth-independent values of a and b_b can be determined accurately from deep measurements of K_∞ and $R_\infty{}^L$ or R_∞. However, if the vertical structure of the waters is unknown, then $K_\infty(z)$ and $R_\infty{}^L(z)$ or $R_\infty(z)$ must be estimated with $K_\infty(z) \approx K_d(z)$ and $R_\infty{}^L(z) \approx R^L(z)$ or $R_\infty(z) \approx R(z)$. For the simulation of Fig. 3, the errors in these approximations at 1 m were −6.2%, −2.7%, and −8.4%, respectively, and at 5 m were −0.95%, −0.66%, and −1.3%. The corresponding profiles of $a(z)$ and $b_b(z)$ are shown in Fig. 4. For the given conditions, the retrieved IOP profiles are accurate at large depths but are in error near the surface. Estimates of $a(z)$ from the E_u–E_d method were slightly better than those from the L_u–E_d method. The errors at 1, 3, and 5 m were −5.7%, −2.2%, and −0.83%, respectively, for the L_u–E_d method and −4.9%, −1.9%, and −0.74% for the E_u–E_d method. Conversely, estimates of b_b obtained from $R^L(z)$ were more accurate than those obtained from $R(z)$, with the errors at the same depths being −8.1%, −3.4%, and −1.4% for the L_u–E_d method and −12%, −4.7%, and −1.9% for the E_u–E_d method.

Near the surface, the percent error in $a(z)$ at a given depth was less than that in either $K_\infty(z)$ or $R_\infty(z)$. This is because the errors in K_∞ and R_∞ were of the same sign near the surface and, as demonstrated in Section 4, the sensitivity coefficients of a with respect to K_∞ (unity) and with respect to R_∞ (Fig. 2) are of opposite signs. Furthermore, estimates of a near the surface were better for the E_u–E_d method than for the L_u–E_d method because the E_u–E_d method gave less-accurate estimates of $R_\infty(z)$, the effects of which better offset those that are due to errors in $K_\infty(z)$. Conversely, because the normalized sensitivity coefficients of b_b with respect to K_∞ and R_∞ are

both positive, the errors in the estimates of b_b were higher than in either K_∞ and R_∞, and estimates of b_b from the L_u–E_d method were better than those from the E_u–E_d method. At large depths, on the other hand, the errors in $K_\infty(z)$ and $R_\infty(z)$ are due primarily to instrument noise and natural variability and are uncorrelated. At these depths, estimates of a still tended to be better than those of b_b because a is less sensitive to R_∞ than is b_b, and the L_u–E_d method tended to slightly outperform the E_u–E_d method for both a and b_b for $\omega_0 > 0.8$ and vice versa for $\omega_0 < 0.8$.

In general, errors in $a(z)$ were due primarily to the errors in $K_\infty(z)$. Because $K_d(z)$ was used to estimate $K_\infty(z)$ for both the L_u–E_d and E_u–E_d methods, the profiles of $a(z)$ obtained from the two methods were similar in both homogeneous and stratified cases. Although $K_u(z) = K_\infty$ at large depths in homogeneous waters, $K_u(z)$ should not be used to estimate K_∞ because internal reflection causes the value of $K_u(z)$ near the surface to be much less than $K_\infty(z)$ and because $E_u(z)$ typically contains more instrument noise than $E_d(z)$ at large depths. The value of $K_L(z, -1)$ on the other hand is much less affected by internal reflection and may be the preferred estimator of K_∞ near the surface if $E_d(z)$ is highly variable because of surface waves.

The accuracy of $a(z)$ and $b_b(z)$ retrieval depended highly on the surface conditions, with the best results occurring when the angular distribution of the light field just below the surface was most near the asymptotic distribution. For example, for the same water conditions as for Figs. 3 and 4 but with diffuse illumination, the estimates of $a(z)$ and $b_b(z)$ were dramatically improved over those shown in Fig. 4. With the L_u–E_d method, the errors in $a(z)$ at 1 and 3 m were only −2.3% and 0.49% (compared with −5.7% and −2.2%), whereas those in $b_b(z)$ at those depths were −3.7% and 0.24% (compared with −8.1% and −3.4%). Likewise, somewhat better estimates of $a(z)$ and $b_b(z)$ were obtained when the sea surface was rough or when the Sun was low in the sky than when the surface was flat or the Sun was at local noon. For example, for the same illumination condition as in Fig. 4 but with 15-m/s winds added, causing a roughened surface, the errors in both $a(z)$ and $b_b(z)$ in the top 5 m were reduced by approximately 6%.

Although the L_u–E_d and E_u–E_d methods for the determination of a and b_b were theoretically derived for homogeneous waters, they can be applied to inhomogeneous waters. If the vertical variation of the IOP's is gradual, it may be possible to determine these profiles accurately, whereas if the vertical structure is fine, only depth-smoothed profiles can be obtained. Figure 5 shows the retrieved profiles of $a(z)$ and $b_b(z)$ for the case of constant $a(z) = 0.3$, $b(z)$ varying sinusoidally between 0.4 and 0.7, a flat surface, and diffuse illumination. It can be seen that $b_b(z)$ is retrieved well below one optical depth. The retrieved $a(z)$ shows sinusoidal error, but its maximum magnitude is only approximately 3%. The case of diffuse illumination is shown in Fig. 5 because

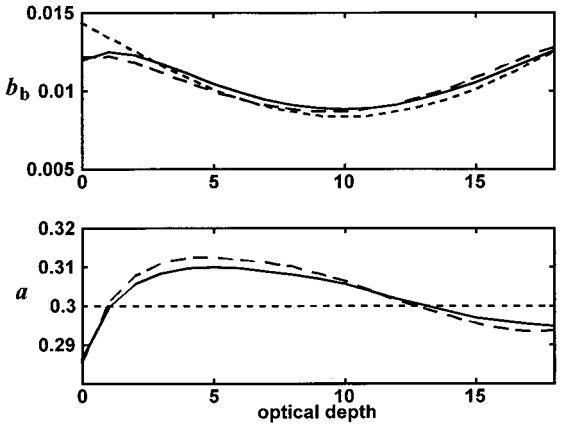

Fig. 5. Determination of the absorption and backscattering coefficients with the L_u–E_d (solid curve) and E_u–E_d (dashed curve) methods for a simulation (dotted curve) with constant $a(z) = 0.3$ and $b(z)$ varying sinusoidally with depth. The surface was flat and the illumination diffuse.

errors that are due to surface effects are minimal, allowing the effects of the stratification to be seen clearly. For a sunny sky illumination, the errors in the estimated $a(z)$ and $b_b(z)$ near the surface are similar to those for the homogeneous case (e.g., Fig. 4), whereas the errors at large depths are similar to those in Fig. 5.

6. Field Experiment

Underwater light and IOP measurements were made on 6 and 8 October 1997 at nine stations in Long Island Sound between the mouths of the Thames and Connecticut rivers. The locations and depths of these sites are given in Table 1. The objective was to compare values of $a(z)$ obtained from the L_u–E_d and E_u–E_d methods with those from a reflecting tube instrument. Verification of $b_b(z)$ values from the light measurements was not possible because there was no independent measurement available.

An upwelling radiance sensor (OCR-200, Satlantic, Inc., Halifax, Nova Scotia) was used to obtain $L_u(z)$ measurements, and a downwelling irradiance sensor (OCI-200, Satlantic, Inc.) was flipped vertically between casts to obtain $E_d(z)$ and $E_u(z)$ alternatively. A data-acquisition system (DATA-100, Satlantic, Inc.) was used to determine the depth and to merge

Table 1. Location and Depth of the Cruise Stations in Long Island Sound

Station Number	Latitude (N)	Longitude (W)	Depth (m)
1	41°16.218′	72°11.711′	29
2	41°19.097′	72°11.195′	5
3	41°50.884′	72°16.970′	7
4	41°14.703′	72°17.175′	32
5	41°15.438′	72°20.008′	8
6	41°15.014′	72°20.568′	8
7	41°13.892′	72°17.901′	41
8	41°13.293′	72°13.585′	50
9	41°17.913′	72°04.975′	9

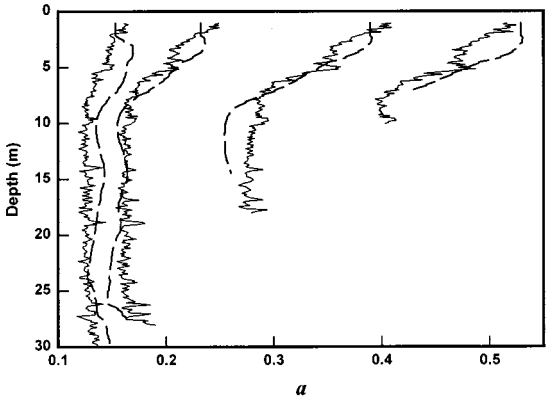

Fig. 6. Comparison at site 8 of estimates of the absorption coefficients at (from right to left) 411, 443, 490, and 555 nm from the ac-9 (solid curve) with those from the L_u–E_d method (dashed curve).

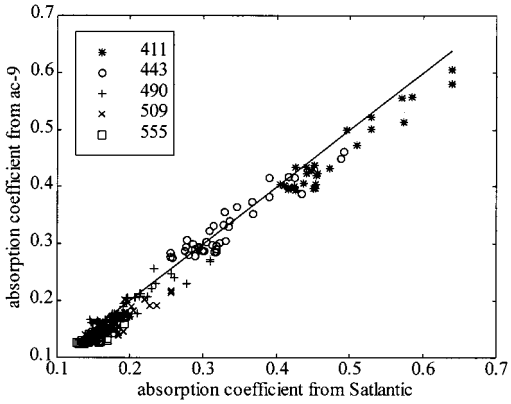

Fig. 7. Absorption coefficients determined with the L_u–E_d method versus those obtained with the ac-9. Included are data at 2-m intervals from sites 1–4 and 7–9. Also shown is the line $a_{\mathrm{Sat}} = a_{\mathrm{ac\text{-}9}}$.

the data streams. At each site, the Satlantic package was deployed twice, once to obtain $E_d(z)$ and $L_u(z)$ and once to obtain $E_u(z)$ and $L_u(z)$. At each wavelength, values of $E_d(z)$ and $K_d(z)$ were obtained at 0.25-m spacing by calculating a least-squares linear fit of $\ln[E_d(z)]$ over a 2-m window centered at each depth. Likewise, values of $E_u(z)$ and $L_u(z)$ were determined at 0.25-m intervals and the ratios $R^L(z)$ and $R(z)$ were formed. At each depth, $R_\infty{}^L$, R_∞, and K_∞ were estimated as the median values of $R(z)$, $R^L(z)$, and $K_d(z)$, respectively, over a 2-m window centered at that depth. Estimates of $a(z)$ were obtained from $R_\infty{}^L(z)$ and $K_\infty(z)$ with the methods described in Section 3 and from $R_\infty(z)$ and $K_\infty(z)$ with the method of Ref. 3.

Profiles of $a(z)$ were also obtained with an ac-9 instrument, with the sensor depth determined with a conductivity, temperature, and depth instrument (Falmouth Scientific, Inc., Cataumet, Massachusetts). At each wavelength λ, estimates of $a_\lambda(z)$ were made by first correcting for temperature effects[14] in the absorption at 715 nm, $a_{715}(z)$, and then correcting for scattering errors[15] at all other wavelengths by subtracting from $a_\lambda(z)$ the term $[a_{715}(z)b_\lambda(z)/b_{715}(z)]$. The contribution of pure water to $a_\lambda(z)$ was added, using the values of Pope and Fry[2] at 412 and 440 nm and those of Tam and Patel[16] for longer wavelengths.

Comparisons of $a_\lambda(z)$ from the Satlantic measurements and from the ac-9 instrument were made at the five shortest Satlantic wavelengths (411, 443, 490, 509, and 555 nm). All stations were characterized by calm seas and clear skies. Four of the sites (1, 4, 7, and 8) were optically deep at all wavelengths, whereas detectable light reached the bottom at the other five sites. A strong current made it impossible to keep the Satlantic instruments in a vertical orientation at station 5.

Shown in Fig. 6 is an example comparison (from site 8) of the estimates of $a_{411}(z)$, $a_{443}(z)$, $a_{490}(z)$, and $a_{555}(z)$ obtained with the ac-9 with those obtained from the L_u–E_d method. The ac-9 data were binned to 0.1-m vertical resolution. Of the wavelengths tested, light at 555 nm penetrated the deepest, providing the longest profiles of $L_u(z)$ and $E_d(z)$. The agreement between the two methods is good, and the gross vertical structure is provided by both methods; however, the natural light field approach can match neither the spatial resolution nor the vertical range of the ac-9.

Shown in Fig. 7 is a scatter plot of the values of the absorption coefficient obtained with the L_u–E_d method, $a_{\mathrm{Sat}}(z)$, versus those obtained with the ac-9, $a_{\mathrm{ac\text{-}9}}(z)$. The values shown are for all stations except stations 5 and 6 and were obtained at 2-m vertical spacing by taking the median value over a 2-m window about each depth. Superimposed in Fig. 7 is the line of perfect correlation, $a_{\mathrm{Sat}}(z) = a_{\mathrm{ac\text{-}9}}(z)$. A linear fit to the data in Fig. 7 yielded a slope of 0.97 and an offset of -0.007, with a correlation coefficient of $r^2 = 0.98$. No consistent trend was determined in the ratio a_{Sat}:$a_{\mathrm{ac\text{-}9}}$ with respect to depth. Meaningful regressions at individual wavelengths were not possible because of the limited range of the values of the IOP's within the data set. A regression of the a_{Sat} and $a_{\mathrm{ac\text{-}9}}$ data for station 5 (in the Connecticut River) yielded a slope of 1.06 and a correlation coefficient of $r^2 = 0.97$; however, these data were not included in Fig. 7 because there was an offset of 0.29 m^{-1}, with $a_{\mathrm{Sat}} > a_{\mathrm{ac\text{-}9}}$. The offset was due presumably to a tilt in the Satlantic package (because of the current) that caused an underestimation of R_∞ and ω_0 and thus an overestimation of $a(z)$. Similarly, the regression of the data at site 6 had a high value of r^2 but was offset by 0.08 m^{-1}.

The L_u–E_d approach was easier to implement than the E_u–E_d method because the $L_u(z)$ signal contained less instrument noise than the E_u signal and the profiles of $L_u(z)$ and $E_d(z)$ were taken simultaneously, whereas the $E_u(z)$ and $E_d(z)$ profiles were done in succession. Nonetheless, the two methods were generally in good agreement. In fact, the estimates of $a(z)$ from the two methods tracked each other closely when the same $K_d(z)$ profiles were used

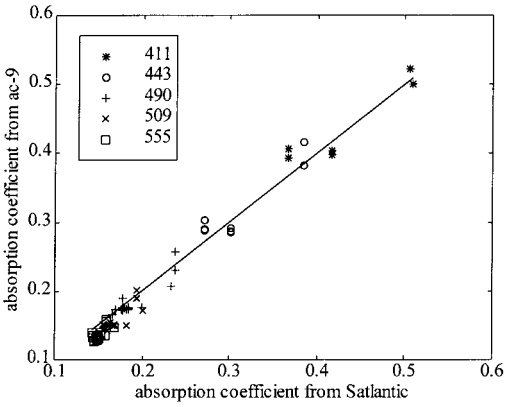

Fig. 8. Absorption coefficients determined with the E_u–E_d method versus those obtained with the ac-9 for sites 1, 4, and 8.

for each. Shown in Fig. 8 is a scatterplot produced in the same manner as Fig. 7 but for the E_u–E_d method at sites 1, 4, and 8. The regression slope, offset, and r^2 values were 1.08, −0.002, and 0.98, respectively.

7. Discussion

A method was proposed for estimating $a(z)$ and $b_b(z)$ from in-water measurements of $L_u(z)$ and $E_d(z)$. This method is valuable because it provides a large-volume measurement of the IOP's that can be used to obtain optical closure with small-volume measurements such as that provided by the ac-9 instrument. The computation of the IOP's is fast, requiring no iteration, and no information about the illumination or surface conditions is necessary.

This method is implemented by first determining $R_\infty{}^L(z)$ and K_∞ and then calculating $a(z)$ and $b_b(z)$ from these values. A sensitivity analysis shows that the estimates of $a(z)$ and $b_b(z)$ are relatively insensitive to errors in $R_\infty{}^L(z)$ and $K_\infty(z)$ and to the assumed scattering phase function. On the other hand, numerical simulations show that the accuracy of estimates of $R_\infty(z)$ and $K_\infty(z)$ depends highly on the illumination conditions, degree of vertical stratification, and the optical depth to which reliable light measurements can be taken.

Optical closure was attempted with measurements in Long Island Sound by comparing values of $a(z)$ obtained with the light measurement approach with those obtained with an ac-9 instrument. The measurements were taken on days with clear blue skies, which numerical simulations suggest are relatively poor conditions for estimating $a(z)$ near the surface from light measurements (because errors in the method that are due to the directional nature of the illumination reach deepest into the water column under sunny conditions). Nonetheless, the agreement between the two methods in the field was good, with estimates of $a(z)$ being systematically larger than those obtained from the ac-9 instrument by only an insignificant amount. In the future, the L_u–E_d method should be compared with ac-9 measurements over a wider range of IOP values than those encountered in our field experiment so that regressions can be made at individual wavelengths.

Application of the natural light field approach proved to be difficult at short wavelengths because of the high light attenuation. The performance of the sensor is therefore important at blue wavelengths.

This research was supported by the U.S. Office of Naval Research. We thank Jeremy Werdell for his help in the collection and processing of the field data. DISORT and Hydrolight were kindly provided by Knut Stamnes and Curtis Mobley, respectively.

References

1. J. R. V. Zaneveld, "A reflecting tube absorption meter," in *Ocean Optics X*, R. W. Spinrad, ed., Proc. SPIE **1302,** 124–136 (1990).
2. R. M. Pope and E. S. Fry, "Absorption spectrum (380–700 nm) of pure water. II. Integrating cavity measurements," Appl. Opt. **36,** 8710–8723 (1997).
3. R. A. Leathers and N. J. McCormick, "Ocean inherent optical property estimation from irradiances," Appl. Opt. **36,** 8685–8698 (1997).
4. H. R. Gordon and G. C. Boynton, "Radiance–irradiance inversion algorithm for estimating the absorption and backscattering coefficients of natural waters: homogeneous waters," Appl. Opt. **36,** 2636–2641 (1997).
5. H. R. Gordon and G. C. Boynton, "Radiance–irradiance inversion algorithm for estimating the absorption and backscattering coefficients of natural waters: vertically stratified water bodies," Appl. Opt. **37,** 3886–3896 (1998).
6. N. J. McCormick, "Analytical transport theory applications in optical oceanography," Ann. Nucl. Energy **23,** 381–395 (1996).
7. S. Chandrasekhar, *Radiative Transfer* (Oxford U. Press, New York, 1950).
8. M. Benassi, R. D. M. Garcia, A. H. J. Karp, and C. E. Siewert, "A high-order spherical harmonics solution to the standard problem in radiative transfer," Astrophys. J. **280,** 853–864 (1984).
9. C. D. Mobley, B. Gentili, H. R. Gordon, Z. Jin, G. W. Kattawar, A. Morel, P. Reinersman, K. Stamnes, and R. H. Stavn, "Comparison of numerical models for computing underwater light fields," Appl. Opt. **32,** 7484–7504 (1993).
10. Z. Tao, N. J. McCormick, and R. Sanchez, "Ocean source and optical property estimation using explicit and implicit algorithms," Appl. Opt. **33,** 3265–3275 (1994).
11. T. J. Petzold, "Volume scattering functions for selected ocean waters," SIO Ref. 72–78 (Scripps Institution of Oceanography, La Jolla, Calif., 1972).
12. Z. Jin and K. Stamnes, "Radiative transfer in nonuniformly refracting layered media: atmosphere–ocean system," Appl. Opt. **33,** 431–442 (1994).
13. C. D. Mobley, "Hydrolight 3.1 Users' Guide, 1996," final report (SRI International, Menlo Park, Calif., 1996).
14. W. S. Pegau, D. Gray, and J. R. V. Zaneveld, "Absorption and attenuation of visible and near-infrared light in water: dependence on temperature and salinity," Appl. Opt. **36,** 6035–6046 (1997).
15. C. S. Roesler and J. R. V. Zaneveld, "High resolution vertical profiles of spectral absorption, attenuation, and scattering coefficients in highly stratified waters," in *Ocean Optics XII*, J. S. Jaffe, ed., Proc. SPIE **2258,** 309–319 (1994).
16. A. C. Tam and C. K. N. Patel, "Optical absorptions of light and heavy water by laser optoacoustic spectroscopy," Appl. Opt. **18,** 3348–3357 (1979).